Optics Letters

# Multiplexing of bias-controlled modulation modes on a monolithic III-nitride optoelectronic chip

Hao Zhang,[1,†] Ziqi Ye,[1,†] Jiabin Yan,[1] Fan Shi,[1] Zhiming Shi,[2] Dabing Li,[2] Yuhuai Liu,[3] Hiroshi Amano,[4] and Yongjin Wang[1,*]

[1]GaN Optoelectronic Integration International Cooperation Joint Laboratory of Jiangsu Province, Nanjing 210003, China
[2]State Key Laboratory of Luminescence and Applications, Changchun Institute of Optics, Fine Mechanics and Physics, Chinese Academy of Sciences, Changchun 130033, China
[3]National Center for International Joint Research of Electronic Materials and Systems School of Information Engineering Zhengzhou University Zhengzhou 450001, China
[4]Institute of Materials and Systems for Sustainability Nagoya University Nagoya 464-8601, Japan
[†]Authors contributed equally to this Letter
[*]wangyj@njupt.edu.cn

Received 15 August 2023; revised 1 September 2023; accepted 2 September 2023; posted 5 September 2023; published 18 September 2023

**III-nitride optoelectronic chips have tremendous potential for developing integrated computing and communication systems with low power consumption. The monolithic, top–down approaches are advantageous for simplifying the fabrication process and reducing the corresponding manufacturing cost. Herein, an ultraviolet optical interconnection system is investigated to discover the way of multiplexing between emission and absorption modulations on a monolithic optoelectronic chip. All on-chip components, the transmitter, monitor, waveguide, modulator, and receiver, share the same quantum well structure. As an example, two bias-controlled modulation modes are used to modulate video and audio signals in the experiment presented in this Letter. The results show that our on-chip optoelectronic system works efficiently in the near ultraviolet band, revealing the potential breadth of GaN optoelectronic integration.**


https://doi.org/10.1364/OL.503429

GaN and other III-nitride compound semiconductors have had a tremendous impact on optoelectronic technology [1,2]. Due to the physical properties of direct transition energy bands and a wide bandgap, III-nitride materials are suitable for manufacturing high-efficiency ultraviolet (UV) emitters and detectors [3]. With the deepening of related research, the quality of III-nitride wafers fabricated on silicon substrate has improved in recent years [4]. The p-doping technique continues to be developed, and considerable progress had been made [5,6]. These advanced technologies are driving the development of UV optoelectronic devices. Monolithic integration of III-nitride optoelectronics is the leading technique to gathering different functional devices on a solid chip [7–9]. There is an overlap between the electroluminescence (EL) spectrum and the responsivity (RS) spectrum of devices with the same quantum well structure, which means that a diode can detect light of a shorter wavelength coming from itself or from other devices with the same structure. Thus, devices with different functions can be made from the same wafer through the same process [10–16]. However, different modulation modes and multiplexing on III-nitride optoelectronic chips remain to be studied.

In this Letter, a monolithic optoelectronic chip was designed and fabricated from a III-nitride wafer based on a silicon to form a micro-lab-on-chip optoelectronic system. The fabrication process does not involve complex postdoping and postgrowth. Emission and absorption modulation modes were developed in order to make full use of on-chip resources. Two modulation modes and multiplexing were fully utilized in an optical interconnection system built on the chip, which contains EL transmitter, electroabsorption modulator, passive waveguide, photodetectors, and off-chip auxiliary circuits. Real-time video and offline music signals were modulated in two different ways, extracted and played effectively.

Figure 1 illustrates the morphology and basic characteristics of the III-nitride optoelectronic chip. The monolithic chip was fabricated from an as-grown wafer on a silicon substrate with a top–down approach. Scanning transmission electron microscopy (STEM) images of the epitaxial layer and the diagram of the fabrication procedure are shown in Figs. S1 and S2 in Supplement 1, respectively. Figure 1(a) shows a detailed structure diagram for each layer of the chip. The step-graded aluminum gallium nitride (AlGaN) buffer layer is often used in conjunction with the aluminum nitride (AlN) nucleation layer as a strain-compensation epitaxial structure to eliminate crack formation in GaN epitaxial films grown on Si [17–19]. The GaN buffer layer can further compensate for the tensile stress, thereby reducing threading dislocations (TDs) and improving crystalline quality. The Si-doped n-type AlGaN layer and the Mg-doped p-type GaN layer are heavily doped for good ohmic contact with metal electrodes. AlGaN/GaN superlattice (SL) cladding layers, p-cladding and n-cladding, could decrease an optical leakage from the chip to the outside. With a GaN-based waveguide as the transmission medium, light travels mainly along the waveguide inside the chip. The low-In-content $In_{0.02}Ga_{0.98}N$ MQW layer acts as both the active layer and the transmission layer. The p-type AlGaN electron blocking layer (EBL) is effective in

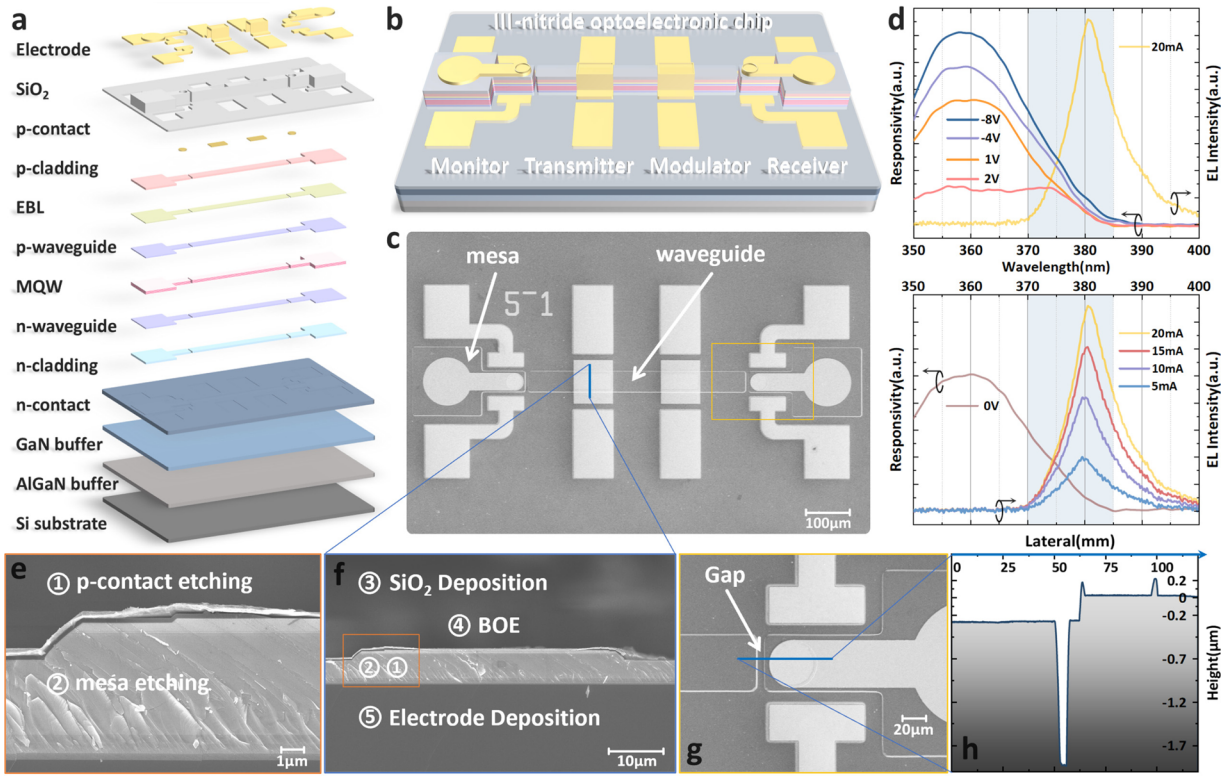


**Fig. 1.** (a) Layered structure of the III-nitride optoelectronic chip. (b) Overall diagram of the chip and four function units. (c) SEM image from the top view. (d) Overlap between the EL and detection spectra under two modulation modes. (e) Local cross-sectional SEM image of the diode. (f) Cross-sectional SEM image of the transmitter and an overview of the process steps. (g) Partial magnification of the isolation trench. (h) Height measurement along the line in (g) with a stylus profilometer.

suppressing overflow electrons above the MQW into the p-type GaN layers [20]. This structure is helpful for realizing planar photonic integrated chips [12,14,21–23].

The overall diagram of our III-nitride optoelectronic chip is shown in Fig. 1(b), including the monitor, transmitter, modulator, and receiver, connected by a straight waveguide. Figure 1(c) is photographed under a scanning electron microscope (SEM, SU8010, Hitachi Corp.) with an accelerating voltage of 5 kV and an emission current of 9.4 $\mu$A. The sizes of the four active regions are two circles with a diameter of 35 $\mu$m, corresponding to the monitor and receiver, and two $90 \times 50$ $\mu$m rectangles, corresponding to the transmitter and modulator. The chip's total size occupies an area of $1030 \times 450$ $\mu$m. Figure 1(d) shows that there is an overlap between the EL and RS spectra of a MQW diode, despite the Stokes shift [24]. The EL and RS spectra were characterized by a high-resolution spectrometer (HR4000, Ocean Insight Corp.) and a quantum efficiency measurement system (Oriel IQE200B, Newport Corp.), respectively. In this overlapping band, 370–385 nm, the light intensity can be modulated by the modulator at different reverse bias voltages, as a result of different levels of electroabsorption [25]. In addition, the transmitter can emit ultraviolet light at various intensities corresponding to injection currents. Different intensities of light can still be further modulated by the modulator. Hence, both the absorption and emission modulation modes can work collaboratively in our optoelectronic chip. Figures 1(e) and 1(f) present sectional SEM images of the transmitter and include annotation providing a brief process overview. The detailed manufacturing process is depicted in Figure S2 in Supplement 1. Figure 1(g) depicts a magnified view of the isolation trench situated between the modulator and receiver, allowing for electrical isolation of the receiver and monitor from other devices. Figure 1(h) shows the height measurement along the line in Fig. 1(g) with a stylus profilometer (DektakXT, Bruker Corp.). The width of the gap is 5 $\mu$m, and the depth of the gap is the same as the mesa etching depth, 1.6 $\mu$m.

Specific electro-optic and photoelectric characteristics of the chip and the signals when two modulation modes work simultaneously are shown in Fig. 2. The I–V curve of the transmitter is shown in Fig. 2(a). The image inset depicts luminescence of the transmitter in a dark field, with an injection current of 10 mA. The light travels predominantly along the waveguide and reflects off the end face of the gap region. Figure 2(b) reflects the photocurrent of the receiver in relation to the reverse bias voltage applied to the modulator, with five distinct constant currents of 0 mA, 5 mA, 10 mA, 15 mA, and 20 mA injected into the transmitter. The absorption change is attributed to the external field-induced quantum confined Stark effect (QCSE) [26,27]. Therefore, it can be utilized to modulate light in the absorption mode. A demonstration of this can be found in Visualization 1. With an increase in the injection current, the intensity of the transmitter's light will rise, and the amplitude of the photocurrent will change more significantly under the same modulation voltage. However, this change does not always increase, which is attributed to the luminous efficiency droop [28]. Photocurrents of the receiver, with a logarithmic scale, are shown in Fig. 2(c), when the transmitter was injected with several different currents, 0 mA, 1 mA, 3 mA, 5 mA, and 10 mA, and the biased

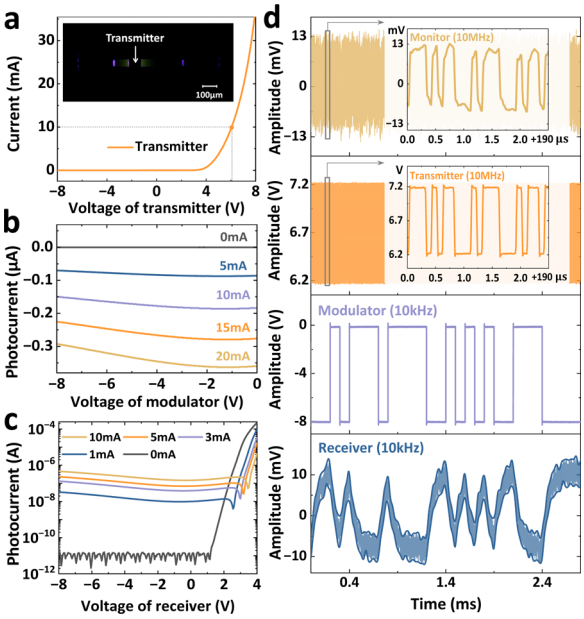


**Fig. 2.** (a) I–V curve and luminous figure of the transmitter. (b) Photocurrent change of the receiver as the voltage biased on the modulator varies with the transmitter under different operating currents. (c) Photocurrents of the receiver versus bias voltages with different injection currents into the transmitter. (d) Multiplexing of 10 MHz emission modulation and 10 kHz absorption modulation with one light source.

voltage on the receiver varying from −8 V to 4 V. At the same bias voltage, for example, 0 V, different injection currents result in different light intensities from the transmitter, and the corresponding photocurrents are formed on the receiver. This mode is often used as an on-chip optical interconnection [29,30].

Figure 2(d) reflects the multiplexing of the emission and absorption modulations in the optoelectronic chip. The transmitter was driven by a pseudorandom binary sequence (PRBS) signal with a pattern length of $2^{11}$-1 (PRBS11), 1 Vpp, biased at 6.7 V, 10 Mbps, and Hi-Z output impedance, from one channel of an arbitrary waveform generator (AWG, 33622A, Keysight Corp.). The modulator was applied by a PRBS11 Hi-Z signal with 8 Vpp, biased at −4 V, from another channel of the AWG. The receiver and monitor were directly connected to the oscilloscope (DSOS604A, Keysight Corp.), with 1 $M\Omega$ input impedance through an AC couple. Signals applied to the transmitter and modulator were tracked by the other two channels of the AWG and sent to the oscilloscope. Although there is some noise, signals of the monitor are mainly determined by the emission modulation and are not affected by the absorption modulator. The two insets in Fig. 2(d) magnify the data of the transmitter and monitor via emission mode with a 10 Mbps PRBS11 signal. The signals of the modulator and receiver were interconnected by absorption modulation at a rate of 10 kHz. It should be noted that the polarity of the received data differs between the two modes. This is because the received data always corresponds to the light intensity, while the final received signals have an opposite polarity due to the characteristics of emission and absorption.

A scheme of the UV interconnection system built on a III-nitride optoelectronic chip is illustrated in Fig. 3. It demonstrates the transmission of the live video via emission modulation and

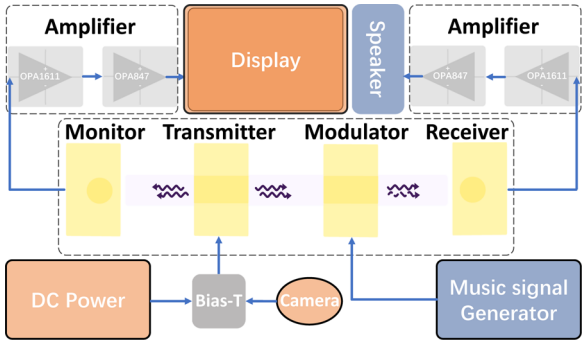


**Fig. 3.** Schematic of the real-time video and music UV interconnection system with multiplexing of the emission and absorption modulations built on a monolithic III-nitride chip.

offline music via the absorption modulation simultaneously. Real-time video information was captured by a commercial camera and loaded onto the transmitter with a DC power through the bias tee. The DC power provides a stable current of 20 mA. The amplitude of the signal coming out of the camera was adjusted to 0.5 Vpp. Music waveform files were prestored in the AWG, so the AWG could generate music signals with 8 Vpp amplitude, bias at −4 Vpp, 8 kSa/s sample rate, and Hi-Z output impedance. Video and music signals were modulated into the transmitter and modulator, with the emission mode and the absorption mode, respectively. In this manner, the utilization of device and modulation resources is maximized. The signals of the photocurrent received and monitored were amplified by a two-stage amplifier and later transferred to the display and speaker. Visualization 2 shows an example of this demonstration.

In order to characterize the modulation rate in each mode, 120 Mbps on-chip data transmission with the emission modulation and 3 Mbps out-of-chip data transmission with the absorption modulation are demonstrated in Fig. 4. In Fig. 4(a), the transmitter was driven by the PRBS11 signal from the AWG with 2 Vpp, 7 V bias voltage, Hi-Z output impedance, default phase state, and 120 MHz frequency. These parameters were synchronized with another channel to trigger the oscilloscope. A clear opening eye diagram appeared on the oscilloscope after a few seconds, as shown in the insets of Fig. 4(a). The absorption modulation test is shown in Fig. 4(b). The transmitter was injected with a stable current of 30 mA from a DC power, so steady UV light travels along the waveguide continuously. The modulator was driven by a 3 MHz PRBS11 signal from the AWG with 8 Vpp, biased at −4 V, and the other parameters were the same as above. A 2 m multi-mode fiber had been used to couple the spot at the gap to a photomultiplier tube (PMT, CR114, Hamamatsu Corp.), with the assistance of a microscope system and a three-axis controlling probe holder. Then, the photocurrent signal is fed into the oscilloscope through a trans-impedance amplifier (TIA, OPA 1611 & 847, TI Corp.). To reduce high-frequency noise interference, the acquisition bandwidth was limited to 5 MHz, and the sampling rate was set to 10 MSa/s. The opening eye diagram indicates that the rate in the absorption modulation mode can reach at least 3 Mbps. The modulation rate should be further improved through more sophisticated processes to fabricate a smaller device.

In summary, a III-nitride optoelectronic chip was fabricated with the monolithic integration method, which dramatically

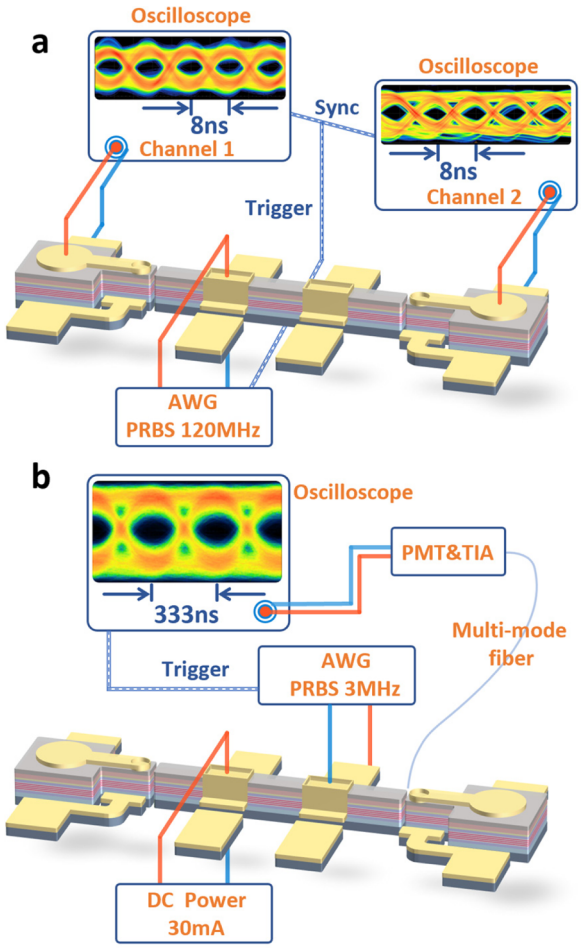


**Fig. 4.** (a) 120 Mbps on-chip data transmission test among the transmitter, receiver, and monitor in the emission modulation mode. (b) 3 Mbps out-of-chip transmission test in the absorption modulation mode.

simplifies the manufacturing process. All devices on the chip, the monitor, transmitter, waveguide, modulator, and receiver, share the same quantum well structure and work effectively in the near UV band. A UV optoelectronic information system was built on this GaN-on-Si chip, and a multimedia on-chip optical communication experiment was carried out. Even with only one light source, the system still work efficiently by multiplexing the emission and the absorption modulations, and it can reduce the cross talk between different signals better than the scheme of multiple light sources. In addition, a total of 120 Mbps on-chip data transmission with emission modulation and 3 Mbps out-of-chip data with the absorption modulation were achieved. The results indicate that it is feasible to integrate electroluminescence, modulation, transmission, and detector components in a monolithic GaN-on-Si chip. Based on this approach and the more advanced III-nitride process, it is promising to develop a large-scale GaN optoelectronic integration in the future.

**Funding.** National Key Research and Development Program of China (2022YFE0112000); National Natural Science Foundation of China (61827804, U21A201550); 111 Project (D17018); Graduate Research and Innovation Projects of Jiangsu Province (KYCX20-0725, KYCX23-1009); Foundation of Jiangsu Provincial Double-Innovation Doctor Program (CZ002SC20021).

**Disclosures.** The authors declare no conflicts of interest.

**Data availability.** All data are available from the authors upon reasonable request.

**Supplemental document.** See Supplement 1 for supporting content.

## REFERENCES

1. H. Amano, Y. Baines, and E. Beam, *et al.*, J. Phys. D: Appl. Phys. **51**, 163001 (2018).
2. H. Amano, R. Collazo, and C. De Santi, *et al.*, J. Phys. D: Appl. Phys. **53**, 503001 (2020).
3. D. Li, K. Jiang, X. Sun, and C. Guo, Adv. Opt. Photonics **10**, 43 (2018).
4. M. Feng, J. Liu, Q. Sun, and H. Yang, Prog. Quantum Electron. **77**, 100323 (2021).
5. P. Pampili and P. J. Parbrook, Mater. Sci. Semicond. Process. **62**, 180 (2017).
6. K. Jiang, X. Sun, Z. Shi, H. Zang, J. Ben, H.-X. Deng, and D. Li, Light: Sci. Appl. **10**, 69 (2021).
7. K. H. Li, W. Y. Fu, Y. Cheung, K. K.-Y. Wong, Y. Wang, K. M. Lau, and H. Choi, Optica **5**, 564 (2018).
8. Q. Wang, G.-D. Yuan, W.-Q. Liu, S. Zhao, L. Zhang, Z.-Q. Liu, J.-X. Wang, and J.-M. Li, Chin. Phys. B **28**, 087802 (2019).
9. J. Yan, L. Wang, B. Jia, Z. Ye, H. Zhu, H. Choi, and Y. Wang, J. Lightwave Technol. **39**, 6269 (2021).
10. Y.-J. Lee, Z.-P. Yang, P.-G. Chen, Y.-A. Hsieh, Y.-C. Yao, M.-H. Liao, M.-H. Lee, M.-T. Wang, and J.-M. Hwang, Opt. Express **22**, A1589 (2014).
11. Y. Wang, X. Wang, B. Zhu, Z. Shi, J. Yuan, X. Gao, Y. Liu, X. Sun, D. Li, and H. Amano, Light: Sci. Appl. **7**, 83 (2018).
12. M. Feng, J. Wang, R. Zhou, Q. Sun, H. Gao, Y. Zhou, J. Liu, Y. Huang, S. Zhang, M. Ikeda, H. Wang, Y. Zhang, Y. Wang, and H. Yang, IEEE J. Select. Topics Quantum Electron. **24**, 8200305 (2018).
13. P. S. Yeh, Y.-C. Chiu, T.-C. Wu, Y.-X. Chen, T.-H. Wang, and T.-C. Chou, Opt. Express **27**, 29854 (2019).
14. H. Zhang, J. Yan, Z. Ye, F. Shi, J. Piao, W. Wang, X. Gao, H. Zhu, Y. Wang, Y. Liu, and H. Amano, Appl. Phys. Lett. **121**, 181103 (2022).
15. H. Zhao, M. Feng, J. Liu, X. Sun, T. Tao, Q. Sun, and H. Yang, Nanophotonics **12**, 111 (2023).
16. R. He, L. Wang, R. Chen, S. Zhang, X. Chen, Z. Yu, J. Liu, J. Wang, and T. Wei, Appl. Phys. Lett. **122**, 021105 (2023).
17. A. Able, W. Wegscheider, K. Engl, and J. Zweck, J. Cryst. Growth **276**, 415 (2005).
18. B. Leung, J. Han, and Q. Sun, physica status solidi (c) **11**, 437 (2014).
19. Y. Sun, K. Zhou, Q. Sun, J. Liu, M. Feng, Z. Li, Y. Zhou, L. Zhang, D. Li, S. Zhang, M. Ikeda, S. Liu, and H. Yang, Nat. Photonics **10**, 595 (2016).
20. H. Hirayama, J. Appl. Phys. **97**, 091101 (2005).
21. C. Shen, T. K. Ng, J. T. Leonard, A. Pourhashemi, H. M. Oubei, M. S. Alias, S. Nakamura, S. P. DenBaars, J. S. Speck, A. Y. Alyamani, M. M. Eldesouki, and B. S. Ooi, ACS Photonics **3**, 262 (2016).
22. C. Shen, C. Lee, E. Stegenburgs, J. H. Lerma, T. K. Ng, S. Nakamura, S. P. DenBaars, A. Y. Alyamani, M. M. El-Desouki, and B. S. Ooi, Appl. Phys. Express **10**, 042201 (2017).
23. M. Xie, Y. Jiang, X. Gao, W. Cai, J. Yuan, H. Zhu, Y. Wang, X. Zeng, Z. Zhang, Y. Liu, and H. Amano, Adv. Eng. Mater. **23**, 2100582 (2021).
24. R. Martin, P. Middleton, K. O'Donnell, and W. Van der Stricht, Appl. Phys. Lett. **74**, 263 (1999).
25. I. Friel, C. Thomidis, and T. Moustakas, J. Appl. Phys. **97**, 123515 (2005).
26. D. A. Miller, D. Chemla, T. Damen, A. Gossard, W. Wiegmann, T. Wood, and C. Burrus, Phys. Rev. B **32**, 1043 (1985).
27. J. S. Weiner, D. A. Miller, and D. S. Chemla, Appl. Phys. Lett. **50**, 842 (1987).
28. J. Cho, E. F. Schubert, and J. K. Kim, Laser Photonics Rev. **7**, 408 (2013).
29. K. H. Li, Y. F. Cheung, W. Y. Fu, K. K.-Y. Wong, and H. W. Choi, IEEE J. Select. Topics Quantum Electron. **24**, 3801706 (2018).
30. X. Ma, Y. Cheung, H. Lyu, and H. Choi, Opt. Lett. **48**, 1124 (2023).